Enhancing Improved Advection Upstream Splitting Method on Triangular Grids: A Hybrid Approach for Improved Stability and Accuracy in Compressible Flow Simulations

Adnan Mohammadi (عدنان محمدی), Mohammad Hassan Djavareshkian* (محمد حسن جوارشکیان)

Department of Mechanical Engineering, Faculty of Engineering, Ferdowsi University of Mashhad, P.O. Box 91775-1111, Mashhad, Iran

Abstract

This paper introduces NAUSM+M+AUFS (New Improved Advection Upstream Splitting Method Plus Artificially Upstream Flux Vector Splitting), a novel hybrid computational scheme for simulating compressible flows on triangular grids. The AUSM+M (Improved Advection Upstream Splitting Method) method is enhanced through two key modifications to boost numerical stability and robustness in high Mach number and hypersonic flows. The first modification redefines the interfacial numerical sound velocity, reducing shock anomalies and improving shock-capturing by integrating velocity and characteristic sound speed parameters. The second modification addresses the insufficiency of the pressure flux dissipation term at supersonic speeds by introducing a formulation that increases dissipation proportionally to the Mach number, thereby enhancing performance in high-speed flows. These enhancements constitute the NAUSM+M method.

The NAUSM+M+AUFS scheme combines the strengths of NAUSM+M and AUFS (Artificially Upstream Flux Vector Splitting) methods, particularly in overcoming the limitations of NAUSM+M in handling shock instabilities and the carbuncle phenomenon on structure triangular grids. A dynamic switching function adjusts the weighting between NAUSM+M and AUFS, optimizing accuracy and stability based on local flow conditions. Numerical tests demonstrate that NAUSM+M+AUFS significantly outperforms AUSM+M, NAUSM+M, and AUFS, effectively eliminating the carbuncle phenomenon and providing smooth shock wave contours. In steady flow analysis, the new hybrid method achieves convergence speeds comparable to AUFS and shows 15% to 45% superior convergence accelerating than AUSM+M, depending on the convergence rate. In addition, in steady flow analysis the accuracy of NAUSM+M+AUFS is 46% better than that of AUFS. This approach represents a significant advancement, offering a robust, accurate, and efficient solution for high-speed aerodynamic simulations, with broad applicability across various compressible flow challenges.

*Corresponding Author: Javareshkian@um.ac.ir

Introduction

Many applications in computational fluid dynamics that deal with compressible flows require highly accurate numerical methods. These methods are crucial for accurately predicting flow phenomenon like shock waves, which feature complex structures. The dominant forces in these inviscid, compressible flows are governed by the compressible Euler equations, which are hyperbolic in nature; these flows are typically addressed using various numerical approaches that originate from the one-dimensional approximate Riemann solver, following the Godunov scheme [1]. Several commonly used approximate Riemann solvers are designed to tackle the Riemann problem, involving a hyperbolic equation with initial conditions that consist of two constants and a discontinuity. Additionally, many numerical approaches have been proposed to solve the Euler equations.

These numerical approaches are primarily categorized into Flux Difference Splitting (FDS) and Flux Vector Splitting (FVS). Within FDS, methods are distinguished based on their wave structure into complete and incomplete approximate Riemann solvers. Complete solvers such as the Roe (Roe approximate Riemann solver) [2, 3], HLLC (Harten Lax van Leer Contact) [4], and Osher [5] schemes are known for their effective handling of contact discontinuities, boundary layers, and steady shocks. However, they are prone to issues like the carbuncle phenomenon or shock instability, particularly in hypersonic vehicles with blunt body designs. Various remedies, such as entropy correction in the Roe scheme [6], have been proposed to tackle these challenges, although they often require arbitrary parameters that can impact shock robustness and may compromise boundary-layer resolution [5].

Incomplete solvers, in contrast, utilize a simplified wave model that omits the linear wave, making them highly stable against carbuncle instability and efficient in capturing strong shocks. These include the two-wave HLL [7] and the one-wave Rusanov [8] solvers. FVS methods [9] are noted for their lower complexity and reduced computational demand as they do not rely on eigen structure data. Similar to incomplete FDS methods [10], FVS approaches provide good shock stability but do not adequately resolve contact discontinuities. To leverage the strengths of both FDS and FVS, Liou and Steffen [11] developed the Advection Upstream Splitting Method (AUSM), which divides inviscid flux into convective and pressure systems. This technique

preserves the shock wave robustness of FVS while ensuring the contact discontinuity accuracy of FDS.

This method is well-regarded for its low dissipation and effective shock management, leading to the development of several new variants like AUSMDV [12], AUSM+[13], and AUSMPW+ [14]. However, challenges remain within the AUSM-family schemes. AUSM+ is particularly sensitive to issues such as pressure variations near walls and excessive numerical values following intense shocks [13, 15]. It also shows limited form of the carbuncle phenomenon [16, 17].

To address the shortcomings of AUSM+ [13], the AUSM+UP [15] has been developed. It achieves high accuracy across various speeds, yet it still encounters the global cut-off issue [18]. Meanwhile, the SLAU (Simple Low Dissipation Advection Upstream Splitting Method) scheme avoids this specific problem and maintains high accuracy at low speeds. However, SLAU also remains susceptible to shock anomalies [19, 20] and generates unphysical outcomes as the Mach number approaches zero [21].

Kitamura et al. [22] presented updated versions of the AUSM-family schemes, including SLAU2 and AUSM+UP2, all of which feature a new pressure flux formulation. SLAU2, an advancement over its predecessor SLAU [23], enhances robustness and performs effectively across a diverse range of Mach numbers. These schemes are distinguished by their high-resolution capabilities. However, they do have some limitations. Notably, SLAU2 are prone to experiencing shock anomalies in scenarios involving strong shocks, particularly in cells characterized by a large aspect ratio [16, 24].

The AUSM+M (Improved Advection Upstream Splitting Method) [25, 26] scheme significantly improves upon its predecessors like AUSM+[27], AUSM+UP [15], SLAU [23], SLAU2, and AUSM+UP2 by addressing specific defects in high Mach number simulations. It introduces a refined velocity diffusion term that incorporates transverse information, crucial for mitigating the carbuncle phenomenon and enhancing shock stability. Moreover, AUSM+M's adjusted numerical sound speed improves the resolution of oblique shocks and effectively distinguishes between entropy-violating expansion shocks and compression shocks, where earlier versions struggled. These improvements make AUSM+M highly effective in handling the complex dynamics of high-speed aerodynamic flows, providing enhanced robustness and accuracy over a range of challenging

conditions. However, it should be noted that the performance of this scheme on triangular meshes has not yet been evaluated.

Kaewta et al. [28] have found that the topology of triangular grids impacts the accuracy and stability of numerical schemes. Triangular grids, while offering significant geometric flexibility in computational fluid dynamics (CFD), often introduce challenges in terms of accuracy and stability. The irregular shape of triangular elements can lead to increased numerical dissipation and dispersion, particularly in high-speed flows where capturing sharp gradients, such as those associated with shock waves is critical. These numerical inaccuracies can propagate through the simulation, leading to distortions in the flow field. Moreover, triangular grids tend to impose stricter stability constraints due to their impact on the eigenvalue distribution of the discretized system [29]. As a result, smaller time steps are often required to maintain stability in explicit time-stepping methods, which can increase computational cost without necessarily enhancing accuracy. Despite these challenges, triangular grids remain indispensable in unstructured mesh generation, particularly when simulating complex geometries such as those found in aerodynamic applications, turbine blades, or high-speed vehicles. Their adaptability to intricate surfaces and boundaries makes them essential, even if some trade-offs in accuracy and stability must be managed.

Quirk [30] proposed a popular hybrid technique to enhance robustness against shock anomalies. This method utilizes a dissipative scheme near shock waves and a more accurate (less dissipative) scheme elsewhere. However, blending these schemes can cause numerical issues, such as smearing of the contact interface or violation of the scheme's positivity. Currently, there is no standard rule for determining the switching parameter between the two schemes that maintains both accuracy and robustness. Thus, researchers have the opportunity to develop an appropriate switching parameter for hybrid schemes that can be applied broadly [27].

AUSM-M+ [31], offers a parameter-free method specifically designed to address the carbuncle phenomenon, a common problem in traditional solvers. While it eliminates the need for empirical adjustments, it has limitations. The third term of the pressure flux function (velocity diffusion term) introduces significant numerical dissipation, which can broaden the shock wave profile. Moreover, the mass flux does not include a pressure difference term. According to Liou [32], mass fluxes containing pressure difference terms tend to exhibit the carbuncle phenomenon. Therefore, it was

expected that removing the pressure difference term would resolve this issue. However, this modification proved ineffective, as the adjusted flux still showed an overshoot at the shock front, underscoring a significant limitation of this approach [23].

Following AUSM-M+, the hybrid SLAU scheme to enhance shock stability and accuracy on unstructured grids [33], but it has several defects. It shows sensitivity to grid type, causing density asymmetries, and abrupt flux function transitions negatively impact convergence. The scheme's performance in diverse flow regimes, particularly those involving complex interactions, requires further validation. Additionally, SLAU's pressure flux calculation deficiencies lead to numerical anomalies and oscillations near shocks, and the imbalance term, can cause further oscillations. The examination of the history of convergence to determine computational costs is also not addressed in the new hybrid SLAU scheme.

The AUSMDV+ scheme [34], which combines elements of AUSMV+ and AUSMD+, was developed to enhance shock stability while attempting to minimize dissipation. However, due to its inherent bias towards the more dissipative AUSMV+ scheme, AUSMDV+ can introduce excessive diffusion, particularly around strong shocks. This additional diffusion can lead to a broadening of shock wave profiles, potentially compromising the accuracy and resolution of complex flow dynamics. Additionally, the scheme's dependency on finely tuned empirical parameters adds complexity, posing challenges for widespread implementation in diverse computational settings.

Roe+ scheme [35], which blends AUSMV+ with the Roe scheme, is a hybrid computational approach that integrates the Roe scheme, known for its accuracy but prone to instabilities like the carbuncle phenomenon, with the robust yet highly dissipative AUSMV+ scheme. This combination is regulated by a novel pressure/density-based weighting switch function, designed to optimally balance dissipation and accuracy. While the scheme enhances stability and maintains accuracy across various tests on triangular grids, it does introduce complexities. These include increased computational demands due to the matrix-based dissipation methods of the Roe component. Additionally, the high level of dissipation through the AUSMV+ can diminish the scheme’s ability to capture sharp features accurately. The ROE+ scheme's performance is also highly sensitive to the accurate calibration of the weighting function parameter, necessitating

careful tuning to adapt to different flow conditions, which may limit its practical applicability without extensive validation.

HLLC+ [36], combines the detailed shock resolution capabilities of HLLC with AUSMV2+ on triangular grids. The HLLC scheme, though accurate, struggles with the carbuncle phenomenon and shock instabilities. The proposed HLLC+ scheme uses a pressure-based detection mechanism to activate the less diffusive AUSMV2+ scheme in regions with significant pressure oscillations, controlled by a new weighting function based on local sound speed ratios. Numerical tests demonstrate that HLLC+ achieves accurate and stable solutions similar to the original HLLC scheme. However, HLLC+ has several shortcomings. The matrix-base dissipation of HLLC scheme can add computational complexity and potential overhead. Additionally, tuning the parameters for the weighting function and detection mechanism can be challenging and may require specific adjustments, limiting the scheme's general applicability and robustness.

To address these challenges comprehensively, the integration of NAUSM+M (New Improved Advection Upstream Splitting Method Plus Artificially Upstream Flux Vector Splitting), with AUFS (Artificially Upstream Flux Vector Splitting) represents a significant breakthrough. New NAUSM+M enhances earlier AUSM-family including AUSM+M [26, 37] variants through two main modifications: the correction of pressure flux and the refinement of sound speed definition. These changes significantly improve the accuracy and convergence of the AUSM+M method. When combined with AUFS[38], which optimizes the calculation of convective and pressure flux components, this new hybrid scheme offers several key improvements: reduced computational overhead by minimizing matrix complexities, making it suitable for complex simulations; enhanced robustness and accuracy by reducing reliance on empirical parameters, thus improving predictiveness and applicability across varied conditions; and improved flexibility and efficiency by addressing the shortcomings of both FDS and FVS methods, providing a more adaptable tool for managing the complex dynamics typical of high-speed aerodynamic flows. This innovative approach not only overcomes the limitations of previous hybrid and matrix-based schemes but also sets a new benchmark in the numerical simulation of compressible flows. By offering a robust, accurate, and efficient solution, the combination of NAUSM+M and AUFS signifies a substantial advancement in computational fluid dynamics, paving the way for more reliable and adaptable methods in analyzing compressible flows. This paper details the development, implementation,

and validation of this hybrid scheme, demonstrating its superiority in various test cases and highlighting its potential for broader application in the field.

2. Governing Equations and inviscid flux computational methods

2.1 Governing Equations

The 2D inviscid equations can be represented in a conservative form as follows:

$$\frac{\partial \boldsymbol{W}}{\partial t}+\frac{\partial \boldsymbol{F}^I}{\partial x}+\frac{\partial \boldsymbol{G}^I}{\partial y}=0 \tag{1}$$

Where W is the conservative vector and $\boldsymbol{F}^I$ and $\boldsymbol{G}^I$ are the inviscid flux vectors:

$$\boldsymbol{W}=\begin{bmatrix}\rho\\ \rho u\\ \rho v\\ \rho E\end{bmatrix}, \boldsymbol{F}^I=\begin{bmatrix}\rho u\\ \rho uu+p\\ \rho vu\\ \rho Eu+pu\end{bmatrix}, \boldsymbol{G}^I=\begin{bmatrix}\rho v\\ \rho uv\\ \rho vv+p\\ \rho Ev+pv\end{bmatrix} \tag{2}$$

In the above equation, ρ , p , (u, v), E are density, static pressure, cartesian velocities, and total energy per unit volume, respectively. The perfect gas equation is defined as follows:

$$p=\rho(\gamma-1)\left(E-\frac{1}{2}(u^2+v^2)\right) \tag{3}$$

2.2. Methods of computing inviscid fluxes

By using the finite-volume methodology, Eq.(1) would be as follows:

$$\frac{d}{dt}\left(\overrightarrow{\boldsymbol{W}}_j\Omega_j\right)+\sum_{k=1}^{3}\overrightarrow{\boldsymbol{H}}_{\boldsymbol{k}}.d\ell_k=0 \tag{4}$$

Where $\overrightarrow{\boldsymbol{H}}\left(\overrightarrow{\boldsymbol{W}}\right)=\overrightarrow{\boldsymbol{F}^I}\left(\overrightarrow{W}\right)i+\overrightarrow{\boldsymbol{G}^I}\left(\overrightarrow{W}\right)j$ is the inviscid flux. Moreover, $\overrightarrow{\boldsymbol{H}}_{\boldsymbol{k}}$ is computed based on the methods of computing inviscid fluxes.

2.2.1 Inviscid flux computing by AUSM+M scheme

$$\vec{H}_k = \left(\frac{\dot{m} + |\dot{m}|}{2}\right)\boldsymbol{\phi_L} + \left(\frac{\dot{m} - |\dot{m}|}{2}\right)\boldsymbol{\phi_R} + p_{1/2}\boldsymbol{N} \tag{5}$$

$$\boldsymbol{\phi} = \begin{bmatrix} 1 \\ u \\ v \\ h \end{bmatrix} \tag{6}$$

$$\boldsymbol{N} = \begin{bmatrix} 0 \\ n_x \\ n_y \\ 0 \end{bmatrix} \tag{7}$$

Here, $p_{1/2}$, $\dot{m}$, h are pressure flux, mass flux, and total enthalpy, respectively.

$$p_{1/2} = \bar{p} - d_p \tag{8}$$

$\bar{p}$ element is defined as the average pressure of two sides of each face. Moreover $d_p$as the dissipation part of pressure flux would be [39]:

$$d_p = \frac{1}{2}(p_L^+ - p_R^-)\Delta p + \mathrm{f}_{1/2}\{(1 - p_L^+ - p_R^-)\bar{p}\} \tag{9}$$

$$\Delta p = p_R\text{-}p_L \tag{10}$$

$$\mathrm{f}_{1/2} = \min\left(1.0, \max\left(\mathrm{f}, \mathrm{M}^2{}_\infty\right)\right) \tag{11}$$

$$\mathrm{f} = 0.5(\,1 - \cos(\pi \mathrm{M})\,) \tag{12}$$

$$\mathrm{M}=\min(1.0, \max(|\mathrm{M_L}|, |\mathrm{M_R}|)) \tag{13}$$

The pressure flux is computed through the below equation [25]:

$$p_{1/2} = \begin{bmatrix} 0 \\ (\bar{p} - d_p)n_x + p_{\mathrm{ux}} \\ (\bar{p} - d_p)n_y + p_{\mathrm{uy}} \\ 0 \end{bmatrix} \tag{14}$$

$$p_{\mathrm{ux}=} \frac{\mathrm{g} \times \gamma \times \bar{p}}{\mathrm{C}_{1/2}} p_L^+ p_R^- (u_\mathrm{R} - u_\mathrm{L}) \tag{15}$$

$$p_{\mathrm{uy}=} \frac{\mathrm{g} \times \gamma \times \bar{p}}{\mathrm{C}_{1/2}} p_L^+ p_R^- (v_R - v_L) \tag{16}$$

$$\mathrm{g} = 0.5(1 + \cos(\pi \mathrm{h}_n)) \tag{17}$$

$$\mathrm{h}_n = \min(\mathrm{h}_\mathrm{k}) \tag{18}$$

$$\mathrm{h}_\mathrm{k} = \min(\frac{p_{Lk}}{p_{Rk}}, \frac{p_{Rk}}{p_{Lk}}) \tag{19}$$

The subscript k indexes all adjacent interfaces between cells i and j for evaluating numerical flux, as illustrated in Figure 1. The function h_n selects the minimum value of h_k and efficiently checks all adjacent interfaces. The normal vectors of each face are n_x and n_y.

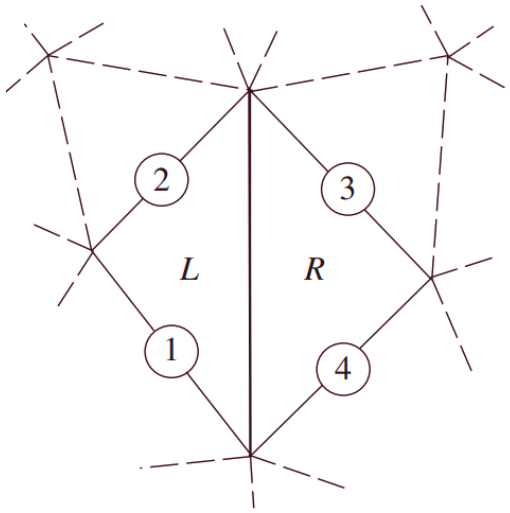

Figure 1. Interface of the cell for evaluating numerical flux

$$p^{\pm}{}_{(L/R)} = \begin{cases} \pm \dfrac{\left(\mathrm{M}_{(L/R)} \pm 1\right)^2}{4} \left(2 \mp \mathrm{M}_{(L/R)}\right) \pm \alpha \mathrm{M}_{(L/R)} \left(\left(\mathrm{M}_{(L/R)}\right)^2 \mp 1\right)^2 & |\mathrm{M}| < 1 \\ \dfrac{\mathrm{M}_{(L/R)} \pm |\mathrm{M}_{(L/R)}|}{2} & |\mathrm{M}| \geq 1 \end{cases} \tag{20}$$

Where:

$$\mathrm{M}_{(L/R)} = \left(V_{(L/R)}\right)/\mathrm{C}_{1/2} \tag{21}$$

$$V_{(L/R)} = u_{(L/R)}.n_x + v_{(L/R)}.n_y \tag{22}$$

$$C_{1/2} = \begin{cases} \dfrac{c^{*2}}{\max(|V_L|, c^*)} & \dfrac{V_L + V_R}{2} \geq 0 \\ \dfrac{c^{*2}}{\max(|V_R|, c^*)} & \dfrac{V_L + V_R}{2} < 0 \end{cases} \quad (23)$$

$$c^{*2} = \frac{2(\gamma - 1)\bar{H}}{(\gamma + 1)} \quad (24)$$

$$\bar{H} = \frac{\gamma RT}{(\gamma - 1)} + \frac{u^2 + v^2}{2} \quad (25)$$

$$\alpha = \left(\frac{3}{16}\right) \quad (26)$$

With "+" and "-" or "L" and "R" symbols, determine the left and right of each face, respectively.

$$\dot{m} = C_{1/2}\, M_{\frac{1}{2}} \begin{cases} \rho_L & M_{1/2} > 0 \\ \rho_R & M_{1/2} < 0 \end{cases} \quad (27)$$

$$M_{1/2} = M_L^+ + M_R^- + (\dot{m})_p \quad (28)$$

$$M_{(L/R)}^{\pm} = \begin{cases} \pm \dfrac{(M_{(L/R)} \pm 1)^2}{4} \pm \dfrac{\left((M_{(L/R)})^2 - 1\right)^2}{8} & |M_{(L/R)}| < 1 \\ \dfrac{M_{(L/R)} \pm |M_{(L/R)}|}{2} & |M_{(L/R)}| \geq 1 \end{cases} \quad (29)$$

$$(\dot{m})_p = \frac{-0.5(p_R - p_L)\,(1 - g)(1 - f)}{\bar{\rho}(C_{1/2})^2} \quad (30)$$

Where, f, $M_{L/R}$, g and $C_{1/2}$ are defined through Eqns.(12),(21),(17), and (23) respectively.

2.2.2. Inviscid flux computing by AUFS scheme

The AUFS approach can be determined as follow [38] :

$$\vec{H}_k = (1 - M)[\tfrac{1}{2}(P_L + P_R) + D_{AUFS}] + M[W^{\beta\_AUFS}(q^{\beta\_AUFS} - s_2)W + P^{\beta\_AUFS}] \quad (31)$$

Where W is the conservative vector defined through Eq.(2) and P vector is defined as follows:

$$P=\begin{pmatrix} 0 \\ pn_x \\ pn_y \\ pq \end{pmatrix} \tag{32}$$

Where q is the normal velocity of an arbitrary interface and is defined as follows:

$$q= un_x + vn_y \tag{33}$$

Note that s_1 and s_2 are two constant scalars. Moreover, M = s_1/ ($s_1 - s_2$), and s_1 , s_2 are the two artificial scalars determining wave speeds. The superscript β classified the left and right direction of waves propagating based on s_1 sign as follow:

$$\beta\_AUFS = \begin{cases} L & for \quad s_1 > 0 \\ R & for \quad s_1 \leq 0 \end{cases} \tag{34}$$

The vector D_{AUFS} is the dissipation of the AUFS scheme and is defined as follows:

$$D_{AUFS} = \frac{1}{2\mathrm{C}_{1/2}} \begin{pmatrix} p_L - p_R \\ (Pu)_L - (Pu)_R \\ (Pv)_L - (Pv)_R \\ \frac{\left(\mathrm{C}_{1/2}\right)^2}{\gamma - 1}(p_L - p_R) + \frac{1}{2}((pq^2)_L - (pq^2)_R) \end{pmatrix} \tag{35}$$

Where:

$$q^2 = u^2 + v^2 \tag{36}$$

The expressions for computing s_1 and s_2 are determined by Sun and Takayama [38] and defined as follows:

$$s_1 = \frac{1}{2}(\mathrm{q}_L + \mathrm{q}_R) \tag{37}$$

$$s_2 = \begin{cases} \min\,(0, q_L - C_L, q^* - c^*) \\ \max\,(0, q_R + C_R, q^* + c^*) \end{cases} \tag{38}$$

Where:

$$q^* = \frac{1}{2}(q_L + q_R) + \frac{C_L - C_R}{\gamma - 1} \tag{39}$$

$$c^* = \frac{1}{2}(c_L + c_R) + \frac{(q_L - q_R)(\gamma - 1)}{4} \tag{40}$$

3. Improvement of AUSM+M scheme

The following subsections focus on improving the accuracy and robustness of the AUSM+M method by introducing a new formulation of interfacial numerical sound velocity and enhancing pressure flux dissipation. A revised definition of sound speed is provided using the AUSMPW+ approach to address deficiencies in hypersonic cases. The new formulation aims to enhance numerical stability and shock capturing by adjusting the interfacial speed of sound, thereby reducing anomalies such as carbuncle. Moreover, improvements to the pressure flux dissipation terms are provided, particularly at supersonic speeds where the original form's dissipation was inadequate. By modifying the dissipation term to increase with the Mach number, the revised approach ensures better numerical accuracy and robustness for high-speed flows.

3.1 New formulation of interfacial numerical Sound velocity

In the AUSM+M method, the sound speed is derived using the AUSMPW+ approach [14]. This offers several advantages: enhanced numerical stability, improved shock robustness, and increased physical accuracy. The AUSMPW+ sound speed effectively resolves normal shocks, captures contact discontinuities, and maintains total enthalpy conservation. However, this sound speed definition lacks robustness in some hypersonic cases [40, 41]. The interfacial speed of sound is crucial for the accuracy and robustness of inviscid flux strategies, especially at high Mach numbers. Properly defining of this term enhances stability and shock capturing by reducing anomalies like carbuncle. Slight modifications in interfacial speed of sound can significantly improve the robustness of the flux schemes. Thus, in the revised version of AUSM+M method (NAUSM+M), the sound speed is defined as follows [40, 41]:

$$C_{1/2} = \begin{cases} \dfrac{c^{*2}}{\max(V_L, c^*)} & \dfrac{V_L + V_R}{2} \geq 0 \\ \dfrac{c^{*2}}{\max(V_R, c^*)} & \dfrac{V_L + V_R}{2} < 0 \end{cases} \quad (41)$$

By applying a mathematical transformation, Eq.(9) can be reformulated as shown below:

$$d_p = \frac{1}{2}(p_L^+ - p_R^-)\Delta p + \frac{3}{4\gamma}\left(\frac{\rho_L + \rho_R}{2}\right) C_{1/2}\,(U_L - U_R) \quad (42)$$

As demonstrated in Eq.(42), the dissipation of the scheme is proportional to the speed of sound. This modification increases the sound speed when (V_L) and (V_R) are negative and greater than (c^*). For instance, if (V_L = V_R= -4) and (c^*= 2), using Eq. (23) results in ($C_{1/2}$ = 4), while using Eq. (42) yields ($C_{1/2}$ = 8). Therefore, this adjustment enhances the robustness of the scheme.

3.2 Improvement of Pressure flux

To enhance clarity, the pressure flux dissipation terms of AUSM+M scheme (Eq.(9)) is represented below:

$$d_p = \frac{1}{2}(p_L^+ - p_R^-)\Delta p + \underbrace{f_{1/2}\{(1 - p_L^+ - p_R^-)\bar{p}\}}_{Inaccurate\ Part} \quad (43)$$

According to this equation, at supersonic speeds (M > 1), the second element of the dissipation term in Eq. (43) becomes constant. Therefore, the numerical dissipation from this term does not change with the Mach number when the speed is supersonic. Numerical analysis shows that this dissipation was insufficient in its original form, and this insufficiency worsens with higher Mach numbers. Therefore, the modified version of dissipation part is provided so that the dissipation increases with the Mach number as follows [22]:

$$d_p = \frac{1}{2}(p_L^+ - p_R^-)\Delta p + \sqrt{\frac{(u_l)^2 + (u_R)^2 + (v_l)^2 + (v_R)^2}{2}}\{(1 - p_L^+ - p_R^-)\bar{\rho}\}C_{1/2} \quad (44)$$

3.3. Establishing a new hybrid scheme: Adjust to structure triangular grids

The following subsections devoted to the development of a new hybrid numerical scheme tailored to enhance the performance of simulations on triangular grids. The scheme aims to address the limitations of previous methods and improve the accuracy, stability, and efficiency of computational fluid dynamics (CFD) simulations, particularly for triangular structure grids. The NAUSM+M scheme is a newly developed AUSM-family numerical method that aims to improve the reliability and accuracy of compressible flow simulations across a wide range of Mach numbers. The NAUSM+M scheme exhibits favorable features like exact resolution of contact discontinuities, preservation of positivity, and damping of numerical overshoots, while avoiding the need for global cut-off strategies required by some earlier AUSM-based methods. The NAUSM+M scheme is known to be accurate on square grid structures; however, inaccurate on triangular grid structures, and its convergence acceleration is also decreased in such grids. To address these limitations, a hybrid technique combining the NAUSM+M scheme with the artificially upstream flux vector splitting (AUFS) scheme is proposed. The AUFS scheme is a new method for solving the Euler equations that splits the flux vector into two parts using two artificial wave speeds, allowing it to capture stationary contact discontinuities and avoid issues like expansion shocks and carbuncle instability that affect many other schemes. A hybrid method is a widely adopted approach that is utilized to enhance the stability of numerical schemes [42, 43]. In general, a hybrid scheme can be represented as follows:

$$\left(\vec{H}_k\right)_H = (1-\beta)\left(\vec{H}_k\right)_D + (\beta)\left(\vec{H}_k\right)_A \tag{45}$$

In the above equation, β represents a weighting function that takes values between 0 and 1, inclusive. The terms $\left(\vec{H}_k\right)_A$ and $\left(\vec{H}_k\right)_D$ illustrate two different types of fluxes: the accurate flux (NAUSM+M) and the dissipative flux (AUFS), respectively. The weighting function β is used to balance the contributions of these two fluxes in the overall equation.

The primary matter in the development of a hybrid scheme lies in the simultaneous achievement of robustness and accuracy through simple and cost-effective means. A common approach is to design the scheme such that the diffusive component is activated in regions of pressure oscillation, such as shock waves, while the accurate component is employed in the remaining regions.

Consequently, the successful realization of this goal necessitates the design and implementation of a robust pressure oscillation detection method and a reliable weighting function within the scheme.

The NAUSM+M+AUFS scheme, built upon the foundation of the accurate a modified AUSM+M scheme (NAUSM+M scheme) and a robust AUFS scheme. A new switching function is utilized [44] to accurately resolve weak nonlinear phenomena and compute strong shock waves. For weak nonlinear phenomena, such as weak shock waves, density discontinuities, and entropy waves a low dissipation scheme (NAUSM+M) is used to reduce numerical dissipation. For strong shock waves, only AUFS is applied. To achieve these goals, a new parameter is introduced to restrict the use of the NAUSM+M scheme near strongly nonlinear regions. This parameter, which is close to 1 in regions of weak nonlinearity and approaches 0 in regions of strong nonlinearity, adjusts the weighting between NAUSM+M and AUFS accordingly.

$$(\beta)_{1/2} = \begin{cases} 1 & \left({}^{d\rho}/_{dx}\right)\left({}^{dp}/_{dx}\right) < 0 \\ \exp\{-(max(1,(\theta)_{1/2}) - 1)\} & \left({}^{d\rho}/_{dx}\right)\left({}^{dp}/_{dx}\right) \geq 0 \end{cases} \tag{46}$$

$$(\theta)_{1/2} = \frac{(\theta^p)_{1/2}}{(\theta^\rho)_{1/2}} \tag{47}$$

$$(\theta^p)_{1/2} = \frac{\max(p_i, p_{i+1})}{\min(p_i, p_{i+1})} \tag{48}$$

$$(\theta^\rho)_{1/2} = \frac{\max(\rho_i, \rho_{i+1})}{\min(\rho_i, \rho_{i+1})} \tag{49}$$

$${}^{dp}/_{dx} = \frac{p_{i+1} - p_i}{\Delta x} \tag{50}$$

$${}^{d\rho}/_{dx} = \frac{\rho_{i+1} - \rho_i}{\Delta x} \tag{51}$$

According to the Rankine–Hugoniot relations, a stronger shock wave results in a higher $(\theta)_{1/2}$. Therefore, if the stencil has a high value of $(\theta)_{1/2}$, the $(\beta)_{1/2}$ parameter should be reduced to avoid using NAUSM+M. Conversely, if the density ratio $(\theta^\rho)_{1/2}$ exceeds the value predicted by isentropic flow or shock waves, $(\theta)_{1/2}$ approaches below 1. In such cases, the cell boundary is likely influenced by weak nonlinear phenomena like weak shock waves, density discontinuities, or entropy wave components. For these stencils, employing NAUSM+M is necessary to achieve a less dissipative solution. Consequently, the $(\beta)_{1/2}$ parameter should be close to one.

4. Numerical Results

This section provides a comprehensive evaluation of several advanced numerical schemes, including AUSM+M, AUFS, NAUSM+M, and NAUSM+M+AUFS, applied to both classical and complex fluid dynamics problems. The goal is to assess the accuracy, robustness, and efficiency of each scheme in capturing intricate flow phenomena across diverse scenarios. The analysis begins with the 1D shock tube problem, where the shock-capturing capabilities and numerical dissipation of the methods are assessed. This is followed by an investigation of hypersonic flow over a stationary circular cylinder, focusing on resolving the carbuncle phenomenon. Next, the Noh problem tests the schemes' performance in handling strong radially symmetric shocks with minimal numerical artifacts. The study then moves to the 2D Riemann problem, which evaluates each scheme's ability to resolve complex shock interactions while maintaining solution symmetry. Finally, the Rayleigh–Taylor instability is examined, providing further insight into the schemes' performance in resolving fluid instabilities and contact discontinuities. Together, these results highlight the strengths and weaknesses of each numerical method, offering valuable insights for advancing computational fluid dynamics (CFD).

4.1. 1D shock tube problem

A one dimensional shock tube is a tube containing two chambers of gas at different pressures, separated by a diaphragm. As a result of the diaphragm rupturing, a shock wave, a contact discontinuity, and a moving expansion wave are generated within the tube [45]. In the problem of the one dimensional shock-tube is investigated on two dimensional domain [0,1]× [0,0.5]. The wall boundary condition is applied to all boundaries. In this problem, the diaphragm is located at position (x=0.5). To discretize the temporal domain of the equations, the dual time-stepping method with a Courant number of 0.9 has been applied.It should be noted that, the results are compared with the exact solution at the dimensionless time (t=0.2136). Also, the domain is discretized into a structured triangular grid by Δx=1/120, Δy= 1⁄160. The initial conditions at the left side of the domain are (ρ_0= 1.0), (u_0= 0.0), and (p_0= 1.0). At the right side of the domain, the initial conditions are (ρ_0 = 0.125), (u_0 = 0.0), and (p_0= 0.1).

Insufficient numerical dissipation along entropy and shear waves can lead to anomlies at the shock interface [46]. It is important to note that shear waves are present only in multidimensional flows [16]. While the dissipation mechanisms of Godunov-based upwind methods effectively dampen disturbances in streamwise direction, they are less successful in managing anomalies that occur transverse to the flow. This deficiency in numerical viscosity can lead to shock instabilities, underscoring the need for improved viscosity strategies transverese the flow, especially in multidimensional contexts. In the case of the one-dimensional Sod-shocktube, the level of numerical viscosity provided is considered adequate for controlling the flow dynamics typical of such configurations. Consequently, based on the limited multidimensional effects and the importance of shear and entropy wave viscosity in multidimensional flows, the performance of methods such as NAUSM+M, AUSM+M, and NAUSM+M+AUFS is similar. Another noteworthy point is that the AUFS method provides smoother and more smeared responses at the critical points of the flow Figure 2, namely the head (B) and tail (C) of an expansion wave, the contact discontinuity (D), and the shock wave (E). An additional crucial point of discussion pertains to the performance integrity of the NAUSM+M+AUFS method in comparison to the AUSM+M method. Despite the application of additional dissipation at the shock locations, the NAUSM+M+AUFS method demonstrates commendable stability and does not exhibit a reduction in accuracy relative to its counterpart .

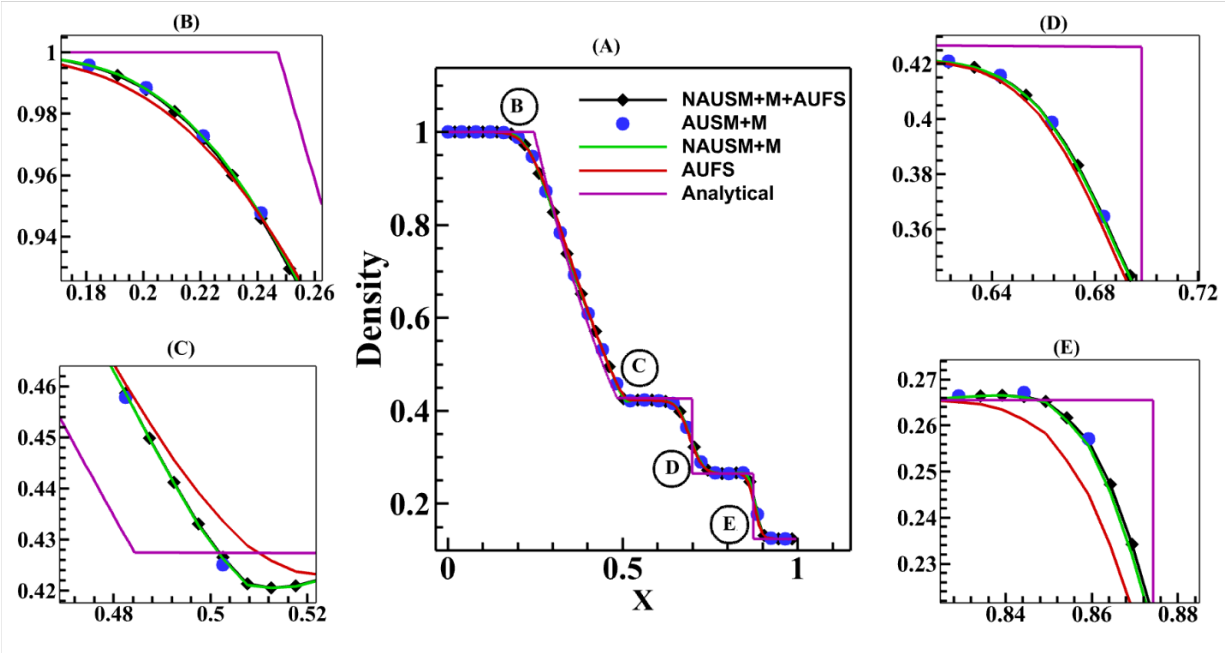

Figure 2. (A) Comparison of density distrubution between various methods along the shocktube (B),(C),(D),(E) Local Enlargement.

4.2. 2D blunt body (steady and super/hypersonic)

The problem involves Mach 8.1 and 3.0, hypersonic flow around a stationary circular cylinder. Peery and Imlay identified an unexpected bump on the bow shock in front of the cylinder, known as the carbuncle phenomenon [47]. Research has shown that accurate shock capturing methods like Roe, HLLC, and AUSM+ often display this carbuncle issue, especially on structured rectangular and triangular grids [36]. Figure 3 shows the computational domain with an inflow boundary on the left and an outflow boundary on the right.

The initial condition is set to $(\rho, u, v, p) = (1.4, 8.1, 0, 1)$. The computations use a first-order accurate method and a Courant number of 0.9. This problem was also examined using two grid sizes with varying aspect ratios.

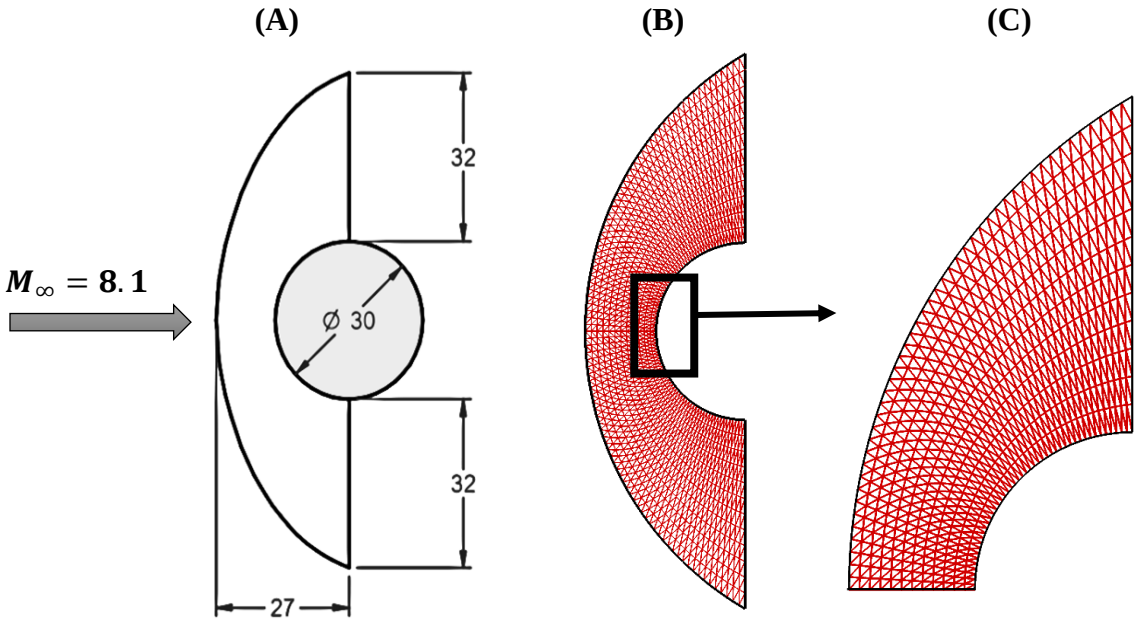

Figure 3: (A) Computational domain (B) Utilized mesh of cylinder (C) Local enlargement mesh cylinder for the Mach number 15 hypersonic flow over a circular cylinder problem[48].

Grid A (Case 1):

The first case was evaluated using a structured triangular grid, A, consisting of 8 intervals in the radial direction and 67 intervals in the circumferential direction. The density contours were calculated using lines ranging from 1.5 to 6, with a step size of 0.28125. The results of the numerical schemes are shown in Figure 4. Figure 4 presents a comparative evaluation of four

numerical schemes—(A) AUSM+M, (B) NAUSM+M, (C) NAUSM+M+AUFS, and (D) AUFS—for simulating a hypersonic flow around a circular cylinder. Each subfigure displays density contours, providing insight into how well each scheme captures shock structures and high-gradient regions in the flow field. In subfigure (A), the AUSM+M scheme reveals significant distortions and unphysical oscillations near the shock, indicative of the carbuncle phenomenon, which compromises the accuracy and stability of the solution in high-speed flows. Subfigure (B) shows an improvement with the NAUSM+M scheme, where the density contours are smoother, and the shock structures are better resolved. However, minor distortions persist near the stagnation zone, limiting the method's accuracy in capturing complex shock interactions. The hybrid NAUSM+M+AUFS scheme in subfigure (C) delivers the most accurate results, with well-resolved shock structures and minimal numerical dissipation. This scheme effectively eliminates the carbuncle phenomenon, providing smooth contours and high fidelity in shock capturing. Finally, subfigure (D) with the AUFS scheme also performs well, though it introduces slightly more dissipation than the hybrid approach, which may slightly impact accuracy in regions with strong shocks.

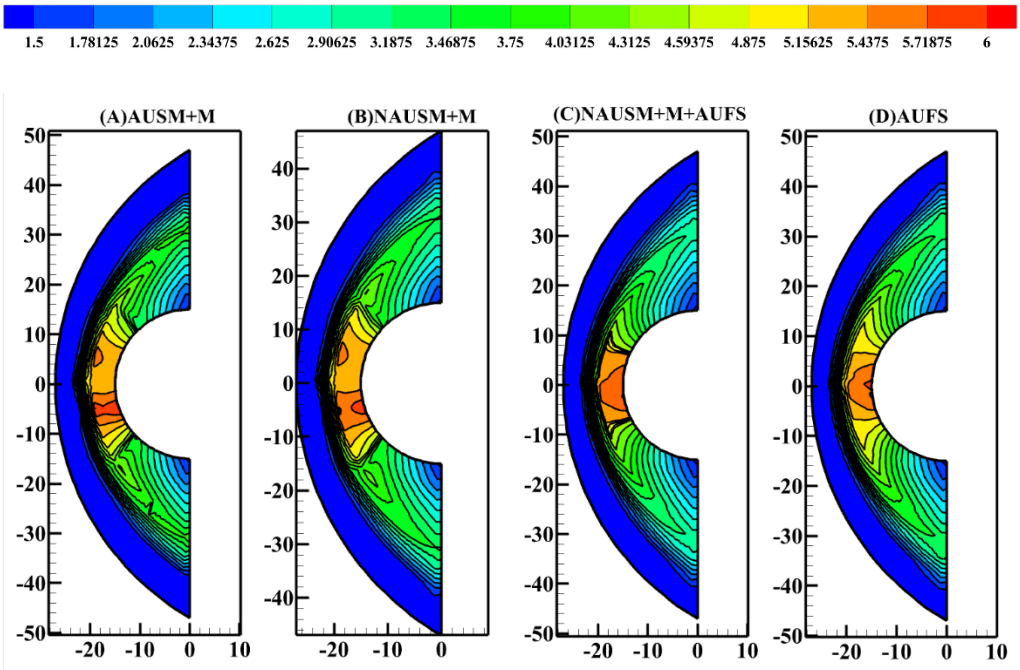

Figure 4: Density for the Mach number 8.1 hypersonic flow over a circular cylinder problem on the structure triangle Coarse grid ((A) AUSM+M, (B) NAUM+M, (C) NAUM+M+AUFS, (D) AUFS).

Figure 5 illustrates the convergence behavior of four numerical schemes—AUSM+M, NAUSM+M, AUFS, and NAUSM+M+AUFS—by comparing the relative convergence speeds in terms of mass residual.

AUSM+M serves as the baseline for convergence, and the NAUSM+M scheme shows a significant improvement, reducing the number of iterations required to reach a residual of -3 by approximately 55% compared to AUSM+M. This improvement indicates better initial convergence speed, though NAUSM+M still lags behind the more advanced schemes. AUFS offers even greater efficiency, achieving a 60% reduction in the number of iterations needed to reach the same residual compared to AUSM+M, marking it as a much faster method at this threshold. The NAUSM+M+AUFS hybrid scheme performs similarly well, showing a 58% improvement in convergence speed over AUSM+M. Although AUFS slightly outperforms NAUSM+M+AUFS in this case, both are considerably more efficient than the baseline.

For deeper convergence at a residual of -6, the performance gaps widen. AUSM+M fails to reach this threshold, highlighting its limitations in achieving high levels of accuracy. NAUSM+M, while capable of reaching a residual of -6, shows a slower convergence compared to the more efficient methods. AUFS, in comparison, improves convergence speed by 21% relative to NAUSM+M, making it significantly more efficient. However, the NAUSM+M+AUFS hybrid scheme demonstrates its superiority once again, converging 15% faster than NAUSM+M and far outperforming AUSM+M, which does not reach this residual level at all.

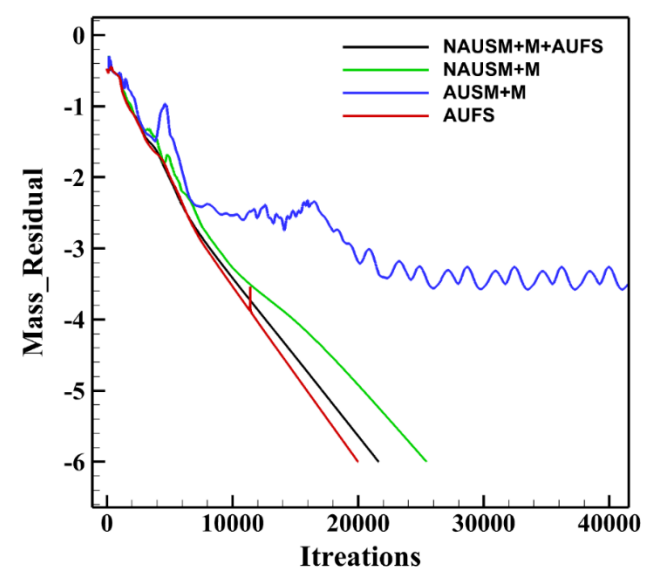

Figure 5: Compare error histroies of hypersonic flow over half-cylinder Coarse grid.

Grid B (Case 2):

The issue was re-evaluated using a structured triangular grid, B, consisting of 12 intervals in the radial direction and 94 intervals in the circumferential direction. Figure 6 is divided into global density contours (subfigures A-D) and local enlargements of the stagnation zone (subfigures E-H), providing a thorough evaluation of each method's ability to resolve complex shock dynamics.

In terms of global density contours, AUSM+M (subfigure A) shows considerable oscillations and unphysical distortions near the shock regions, a clear indication of the carbuncle phenomenon affecting its accuracy and stability. NAUSM+M (subfigure B) reduces these oscillations through Eqs. (41),(44) and improves the overall smoothness of the contours, though some minor distortions persist, particularly in areas of high gradient. The hybrid NAUSM+M+AUFS scheme (subfigure C) significantly outperforms both AUSM+M and NAUSM+M, effectively eliminating the carbuncle phenomenon and producing smooth, well-resolved shock structures with minimal numerical dissipation. AUFS (subfigure D) also demonstrates good shock-capturing capabilities but introduces slightly more dissipation compared to NAUSM+M+AUFS, leading to a small decrease in overall accuracy.

The local enlargements around the stagnation zone provide a more detailed view of how each method handles critical regions like stagnation zone. AUSM+M (subfigure E) reveals significant distortions near the stagnation point, underscoring the scheme’s limitations in managing complex shock interactions. NAUSM+M (subfigure F) improves accuracy in this region, though subtle artifacts remain. In contrast, NAUSM+M+AUFS (subfigure G) demonstrates superior performance, with minimal distortions and smooth transitions, capturing the shock interactions with high fidelity. AUFS (subfigure H) shows reliable shock capturing but introduces slightly more dissipation than the hybrid scheme, which could affect precision in highly dynamic regions.

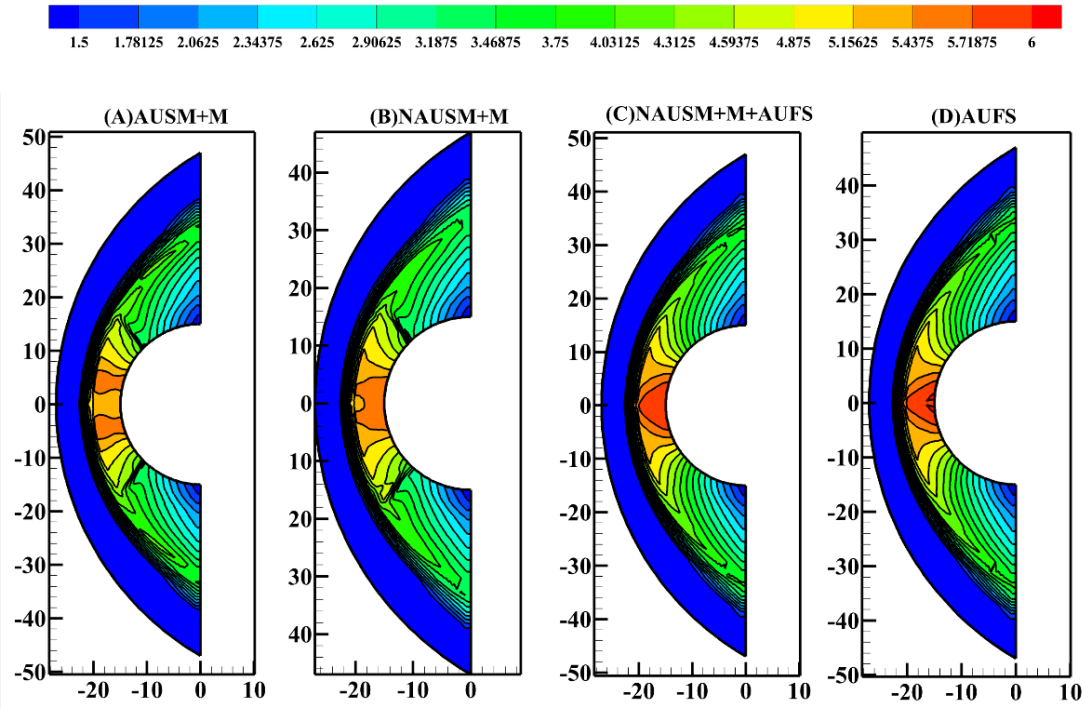

a) Density contours ((A) AUSM+M, (B) NAUM+M, (C) NAUM+M+AUFS, (D) AUFS)

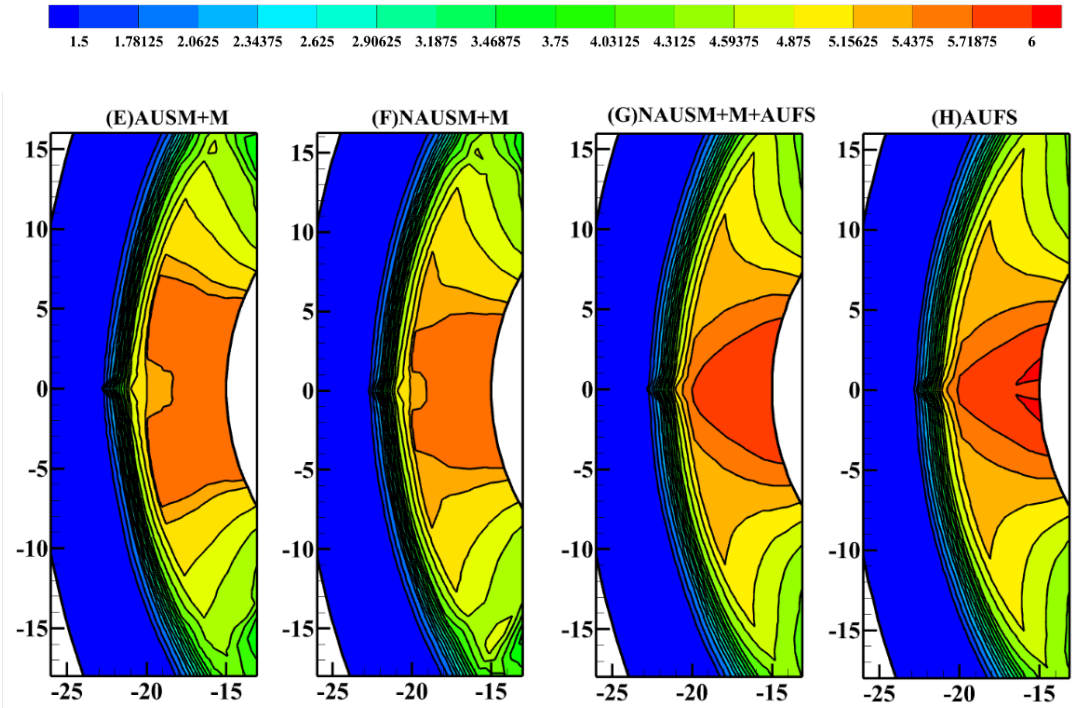

b) Local Enlargement ((E) AUSM+M, (F) NAUM+M, (G) NAUM+M+AUFS, (H) AUFS)

Figure 6: Density for the Mach number 8.1 hypersonic flow over a circular cylinder problem on the structure triangle grid (a)Density contours (b) Local Enlargement of density contours around stagnation zone.

Figure 7 provides a comparative analysis of the aforementioned schemes. It is evident that NAUSM+M+AUFS and AUFS exhibit the fastest convergence rates compared to the other two methods. Notably, while the convergence processes of AUSM+M and NAUSM+M encounter stall after a definite number of iterations, NAUSM+M+AUFS and AUFS achieve complete convergence. In a detailed examination of mass residuals at 20,000 iterations, AUFS emerges as the most efficient, with the lowest residual of -5.0, reflecting its rapid convergence and reduced computational demands. NAUSM+M+AUFS closely follows with a residual of -4.8, indicating a slightly higher computational cost but similarly efficient convergence. In contrast, AUSM+M and NAUSM+M show slower convergence with residuals of -2.5 and -2.0 respectively.

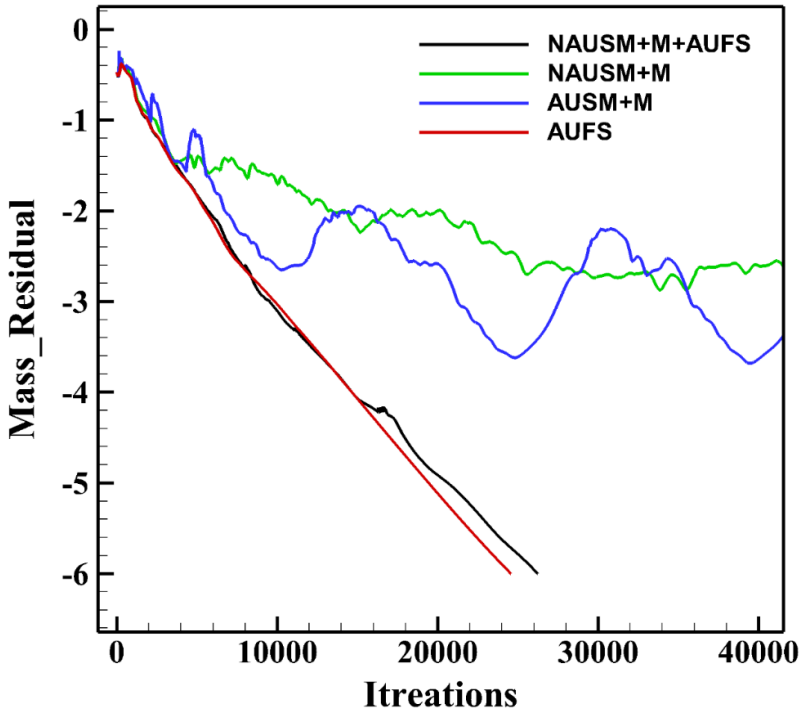

Figure 7: Compare error histroies of hypersonic flow over half-cylinder.

According to the above comparative analysis, it has been determined that the AUFS and NAUSM+M+AUFS methods exhibit superior performance in terms of accuracy and convergence rate compared to other numerical schemes. Consequently, to furnish a more comprehensive comparison, Table 1 presents a detailed evaluation of these two numerical methods. According to this table, NAUSM+M+AUFS displays superior accuracy and closer alignment with analytical solutions compared to AUFS across different Mach settings. For Mach 3, while AUFS underestimates the pressure by -1.84%., NAUSM+M+AUFS nearly matches the analytical values

with a slight overestimation of +0.29%. At Mach 8.1, the situation demands a greater numerical dissipation to prevent numerical anomlies and non-physical responses like the carbuncle phenomenon due to stronger shock conditions. AUFS overestimates the pressure by 6.29%, whereas the new numerical scheme, NAUSM+M+AUFS, closely aligns with the analytical values, with an overestimation of only 4.3%. This indicates that the new hybrid numerical scheme is 46% more accurate than the AUFS scheme at Mach 8.1. NAUSM+M+AUFS offers a balanced level of numerical dissipation that effectively addresses the accuracy and convergence issues seen in AUSM+M and NAUSM+M, while also maintaining lower dissipation levels compared to AUFS, particularly at contact discontinuities where AUFS exhibits high dissipation rates.

Based on the above hypersonic investigation, AUSM+M, while effective, demonstrates notable sensitivities to numerical instabilities and a propensity for unphysical results in shock regions. NAUSM+M improves on this by reducing such anomalies and enhancing shock capturing capabilities, though it still exhibits shock anomlies and stall in convergence rate. NAUSM+M+AUFS stands out as the most balanced method, effectively eliminating the carbuncle phenomenon, demonstrating high accuracy close to analytical solutions, and showing rapid convergence with minimal computational demand. This method strikes an optimal balance between accuracy and dissipation, adeptly handling strong shock conditions with considerable finesse. In contrast, AUFS, although it provides good shock control and stability, tends to be overly dissipative, particularly in handling shear waves, which leads to underestimations that might compromise the accuracy. Overall, NAUSM+M+AUFS presents the best performance across the metrics of stability, accuracy, convergence rate, and numerical dissipation.

Table 1: Pressure after shock; comparisons in Mach 3 and 8.1 blunt-body tests.

$\boldsymbol{P_2/P_\infty}$	NAUSM+M+AUFS	AUFS	Analytical
$\boldsymbol{M = 3.0}$	10.36	10.14	10.33
$\boldsymbol{M = 8.1}$	73.22	71.85	76.37

While numerical stability and accuracy are essential in the development of numerical schemes, computational efficiency must also be considered to ensure a fast solver capable of handling large-scale industrial problems. The computational resources for this study were as follows: all simulations were conducted on a Lenovo computer equipped with an Intel Core i5-6200U processor, 8 GB of RAM, and running Windows 10 Professional.

Table 2 presents the CPU time required by each of the four schemes to solve the problem. The AUFS scheme was identified as the fastest among the evaluated methods, serving as the baseline for computational efficiency. Its rapid computational speed makes it suitable for applications requiring quick results. However, this efficiency comes at the expense of accuracy; the AUFS scheme is 46% less accurate than the hybrid NAUSM+M+AUFS scheme. This trade-off suggests that while AUFS is effective for preliminary analyses or scenarios where speed is prioritized over precision, it may not be adequate for simulations demanding high-fidelity results.

The NAUSM+M+AUFS hybrid scheme combines the strengths of both the NAUSM+M and AUFS schemes, achieving a substantial improvement in accuracy with only a moderate increase in computational time—approximately 24% more CPU time than the AUFS scheme at a mass residual of 10^{-6}. Importantly, the hybrid scheme successfully reaches the tighter convergence criterion of a mass residual of 10^{-6}, demonstrating its robustness and reliability. This balance of efficiency and accuracy makes it well-suited for industrial applications where accurate modeling of complex flow phenomena is critical, and computational resources are limited.

Notably, the NAUSM+M and AUSM+M schemes did not achieve the tighter convergence criterion of a mass residual of 10^{-6}, stalling around 10^{-2}. This inability to reach higher convergence levels indicates potential issues with numerical stability or convergence behavior inherent in these schemes. At a mass residual of 10^{-2}, the NAUSM+M scheme required 112 units of CPU time, which is 160% more than the AUFS scheme, rendering it impractical for large-scale or time-sensitive simulations. The AUSM+M scheme, while more efficient than NAUSM+M, still required 34% more CPU time than AUFS and similarly failed to reach the tighter convergence threshold.

The stalling of NAUSM+M and AUSM+M around a mass residual of 10^{-2} underscores their limitations in achieving high levels of convergence and accuracy. This behavior suggests that these schemes may struggle with numerical challenges such as handling strong shocks or complex flow features typical in hypersonic flows through triangular grids.

The impact of convergence criteria on computational performance is significant. Tighter convergence thresholds inherently demand more computational effort due to the increased number of iterations required. The varying ability of each scheme to reach these thresholds highlights the importance of selecting appropriate numerical methods based on the specific accuracy requirements and computational constraints of a simulation. The NAUSM+M+AUFS scheme's success in achieving a mass residual of 10^{-6} demonstrates its superior convergence properties compared to the other schemes.

The analysis highlights the inherent trade-offs in CFD simulations among computational efficiency, accuracy, and convergence behavior. The NAUSM+M+AUFS hybrid scheme effectively balances these factors, achieving high accuracy and convergence levels with a relatively modest increase in computational cost. Its performance demonstrates the potential of hybrid methods to enhance solution accuracy and robustness without excessively compromising efficiency. For practical applications—especially in industrial settings where accuracy and reliability are paramount—the hybrid scheme offers a viable and advantageous solution.

Table 2: Comparison of CPU time for hypersonic flow over half-cylinder.

Scheme	Mass Residual= (10^{-6})		Mass Residual= (10^{-2})	
	CPU Time(s)	**%Over AUFS**	**CPU Time(s)**	**%Over AUFS**
NAUSM+M+AUFS	235	24	53	23
AUFS	190	----	43	-----
NAUSM+M	---	----	112	160
AUSM+M	---	----	58	34

4.3. Noh problem

The problem is modeled on a domain ((x, y) $\in$[0, 1] ×[0, 1]), with an initial density of 1 and pressure set to zero ((1×10^{-6} to avoid numerical issues). The initial velocity is directed from the origin with a constant magnitude of 1. The solution features an infinitely strong, circularly symmetric shock originating from the origin. Within the shock (inside the circle), the density is 16, the velocity is zero, and the pressure is (16/3). The shock speed is (1/3), and ahead of the shock, the density is $(1 + \frac{t}{\sqrt{x^2+y^2}})$, while the velocity and pressure remain as initially set [48]. The

simulation uses wall boundary conditions on the left and bottom boundaries, with the exact solution enforced on the top and right boundaries. The simulation runs until (t = 2) on the grid: (400 ×400). Many schemes fail with this problem, and those that succeed often show numerical artifacts [49]. The provided density contour figures (A-D) and their zoomed-in views (E-H) allow for a comprehensive comparison of the methods AUSM+M, NAUSM+M, AUFS, and NAUSM+M+AUFS to clarify the modifications and determine the optimal scheme for the Noh problem (Figure 8). AUSM+M (A) serves as the baseline method, presenting the fundamental structure of the shock wave. However, its zoomed-in view (E) reveals numerical artifacts and less smooth transitions, indicating limitations in accuracy and stability. NAUSM+M (B) demonstrates significant improvements over AUSM+M, with a more stable manner specefically in origin zone . The zoomed-in view (F) highlights these enhancements, showcasing smoother transitions and fewer artifacts, thereby reflecting better numerical stability and handling of complexities in Noh test case. AUFS (C) offers an alternative manner, while this method exhibits some improvements over AUSM+M in the overall density contour, the zoomed-in view (G) still displays a number of artifacts. The combined method, NAUSM+M+AUFS (D), integrates the strengths of both NAUSM+M and AUFS. This results in a superior representation of the shock wave, merging the stability and accuracy of NAUSM+M with the advanced stability techniques of AUFS. The zoomed-in view (H) reveals the least artifacts and the smoothest transitions among all methods, indicating that NAUSM+M+AUFS captures high gradient and critical zones with the highest accuracy and minimal numerical artifacts.

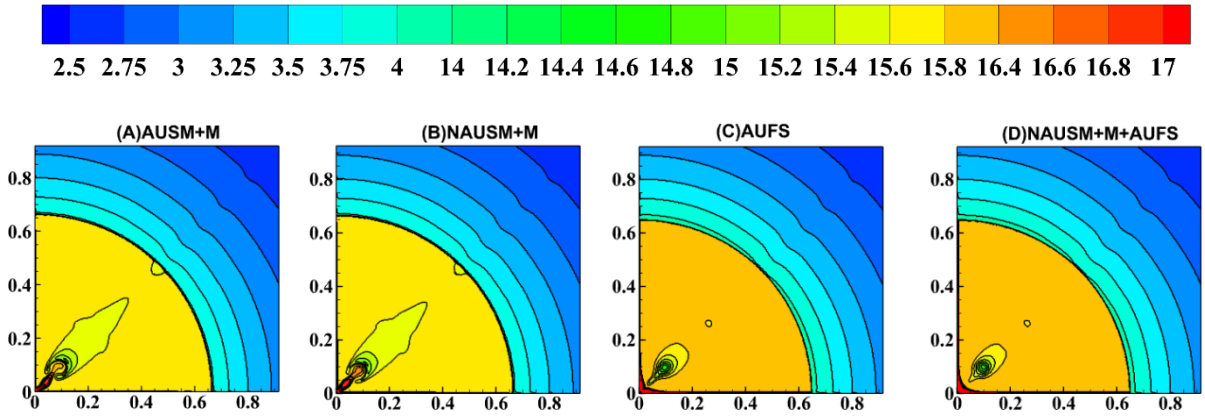

a) Density contours ((A) AUSM+M, (B) NAUM+M, (C) AUFS, (D) NAUM+M+AUFS)

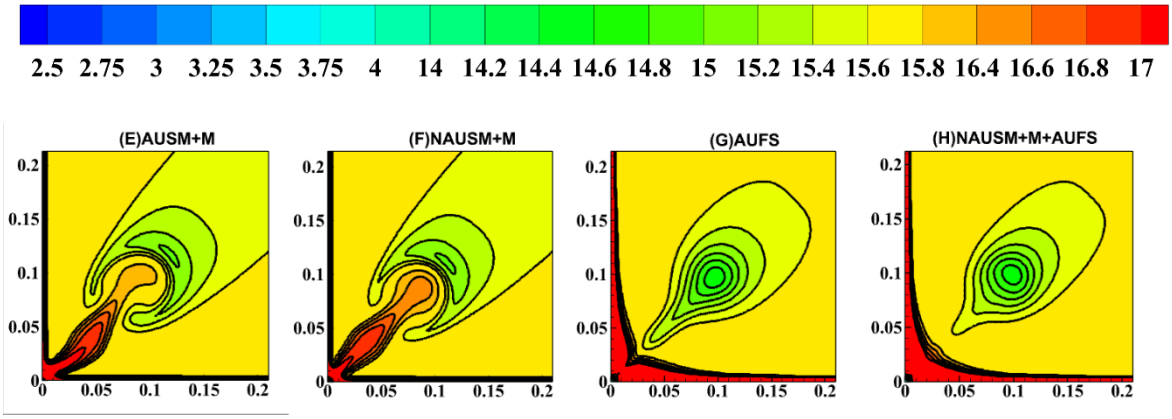

b) Local Enlargement around the shock wave ((E) AUSM+M, (F) NAUM+M, (G) AUFS, (H) NAUM+M+AUFS)

Figure 8: (a) Density contours of Noh problem (from 2.5 to 4.0 in step of 0.25, and 14.0 to 17.0 in step of 0.2)
(b) Local Enlargement of density contours around the shock wave.

The computational performance of the numerical schemes for the Noh problem at (t = 2.0) seconds, as presented in ***Table 3***, offers critical insights into their efficiency and suitability for large-scale simulations.

The NAUSM+M+AUFS hybrid scheme demonstrates a clear advantage by offering significant accuracy improvements with only a minimal increase in computational cost. The 3% increase in CPU time over AUFS is marginal, especially considering the enhanced ability to accurately capture high-gradient regions and critical flow features without numerical artifacts.

In contrast, NAUSM+M and AUSM+M require substantially more CPU time—58% and 38% increases over AUFS, respectively—yet do not provide commensurate improvements in accuracy when compared to NAUSM+M+AUFS. While NAUSM+M shows better accuracy than

AUSM+M, its high computational cost remains a concern. AUSM+M, despite its significant CPU time, exhibits numerical artifacts similar to those in AUFS, indicating that the additional computational effort does not translate into better accuracy.

The AUFS scheme, while being the most computationally efficient, shows limitations in accuracy as evidenced by the presence of numerical artifacts in critical regions. This suggests that AUFS may not be sufficient for simulations where precise modeling of shock waves and high-gradient areas is necessary. Integrating the analysis of computational costs with accuracy considerations, the NAUSM+M+AUFS scheme emerges as the optimal choice for simulating the Noh problem. It achieves high accuracy and numerical stability, effectively capturing complex flow features with minimal numerical artifacts, all while maintaining computational efficiency comparable to the AUFS scheme.

Table 3: Comparison of CPU time at time=2.0s for Noh problem.

Scheme	CPU Time(s)	%Over AUFS
NAUSM+M+AUFS	2323	3
AUFS	2251	----
NAUSM+M	3115	58
AUSM+M	3555	38

4.4 Two-dimensional Riemann problem

The two-dimensional Riemann problems documented in [50] have established themselves as fundamental benchmarks for assessing schemes designed to solve the compressible Euler equations.

The two-dimensional Riemann problem test case can be conducted through different possible configurations of shock waves, rarefaction waves, and slip lines in the solution of two-dimensional Riemann problems for gas dynamics. These configurations represent distinct patterns of how waves interact at the interfaces between different quadrants of initial data in the problem. Each configuration corresponds to a particular combination of physical wave types (shocks, rarefactions, or slip lines) and their interactions. In this investigation, one address the third configuration of the Riemann problem, which describes the interaction of four shock waves within the domain $[0, 1] \times [0, 1]$.

Outflow boundary conditions are imposed uniformly, and The initial conditions of the two-dimensional Riemann problem are illustrated in (Figure 9), showing the configuration of the four distinct states within the computational domain.

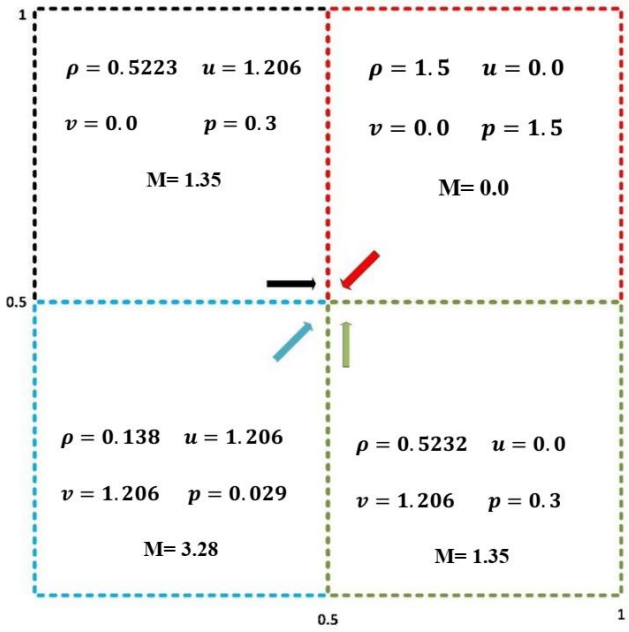

Figure 9: Initial condition of two-dimensional Riemann problem (configuration3).

As mentioned in reference [50], it is crucial that the solution to this problem maintains symmetry along both the northeast and southwest diagonals consistently. The symmetry of the solution indicates that the numerical method has successfully captured the physical behaviors of the flow with higher accuracy and fewer non-physical artifacts. However, schemes with insufficient rate of dissipation often fail to preserve this symmetry. This issue arises from the accumulation of systematic rounding errors. To assess the performance of the selected schemes—AUSM+M, NAUSM+M, and NAUSM+M+AUFS—Figure 10 presents a comparative analysis of their density contours at t=0.3. Subfigures A, B, and C display the global density contours for each scheme: AUSM+M, NAUSM+M, and NAUSM+M+AUFS, respectively. Subfigures D, E, and F show enlarged views of critical regions, allowing for a detailed examination of the flow structures where shock interactions occur. These enlargements provide additional clarity on how each scheme handles the resolution of complex shock dynamics and the preservation of flow symmetry.

In subfigure (A), the AUSM+M scheme shows clear signs of asymmetry, especially in regions of shock interactions. The density contours are distorted, suggesting that the scheme introduces

numerical dissipation that is insufficiently controlled. This lack of dissipation management leads to visible numerical artifacts, most notably in the triangular structures near the shocks, which are more apparent in the enlarged view shown in subfigure (D). These artifacts result from the accumulation of rounding errors, indicating that AUSM+M struggles to preserve the necessary symmetry along the diagonals. Although AUSM+M effectively captures shocks, its inability to maintain flow symmetry and control dissipation limits its accuracy in this context.

In contrast, subfigure (B) shows the results from the NAUSM+M scheme, which improves upon AUSM+M by reducing numerical dissipation. The density contours in subfigure (B) are more symmetric compared to those in subfigure (A), with fewer distortions. However, as seen in the enlarged view (subfigure (E)), subtle asymmetries persist in regions of intense shock interaction. While NAUSM+M provides better control over dissipation, its performance is not yet optimal, as small artifacts remain. These artifacts, though reduced, still affect the accuracy of the flow solution, particularly in highly dynamic regions where shocks are interacting.

The most significant improvement is observed in subfigure (C), where the NAUSM+M+AUFS scheme produces highly symmetric density contours, with minimal numerical artifacts. The enlarged view in subfigure (F) confirms that the scheme handles shock interactions with great precision, preserving the fine details of the flow. The enhanced dissipation control provided by the AUFS modification plays a crucial role in this result, as it effectively manages rounding errors and numerical dissipation. Consequently, NAUSM+M+AUFS not only maintains symmetry along the diagonals but also captures the complex shock dynamics with high fidelity. This performance makes it the most accurate and reliable scheme among the three.

Moreover, the comparison of the global density contours (A-C) and their enlarged counterparts (D-F) highlights the strengths and weaknesses of each scheme. AUSM+M exhibits noticeable asymmetry due to insufficient dissipation control, leading to inaccuracy in the solution. NAUSM+M offers an improvement by reducing these artifacts, but it still falls short in highly dynamic regions. Finally, NAUSM+M+AUFS demonstrates superior performance, achieving both high symmetry and accurate shock capturing, making it the most suitable scheme for solving the two-dimensional Riemann problem

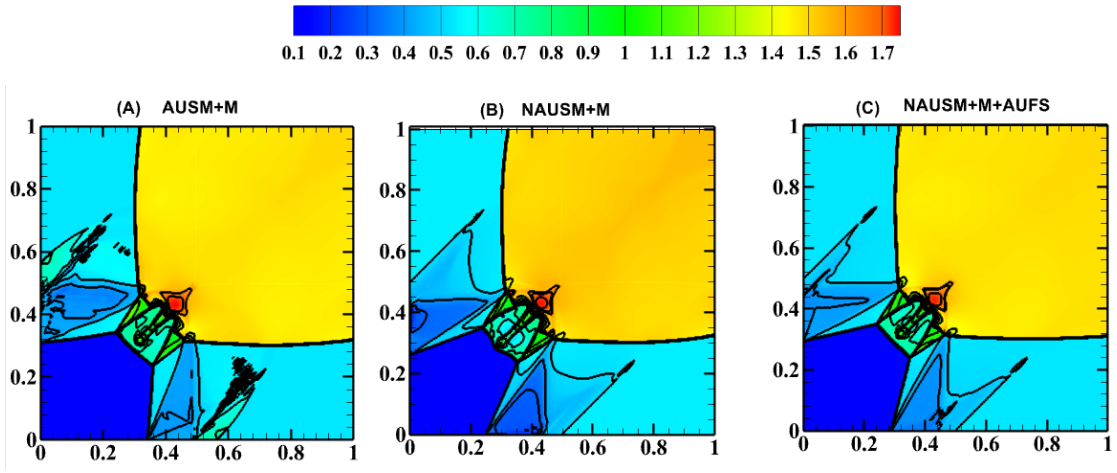

a) Density contours ((A) AUSM+M, (B) NAUM+M, (C) NAUM+M+AUFS).

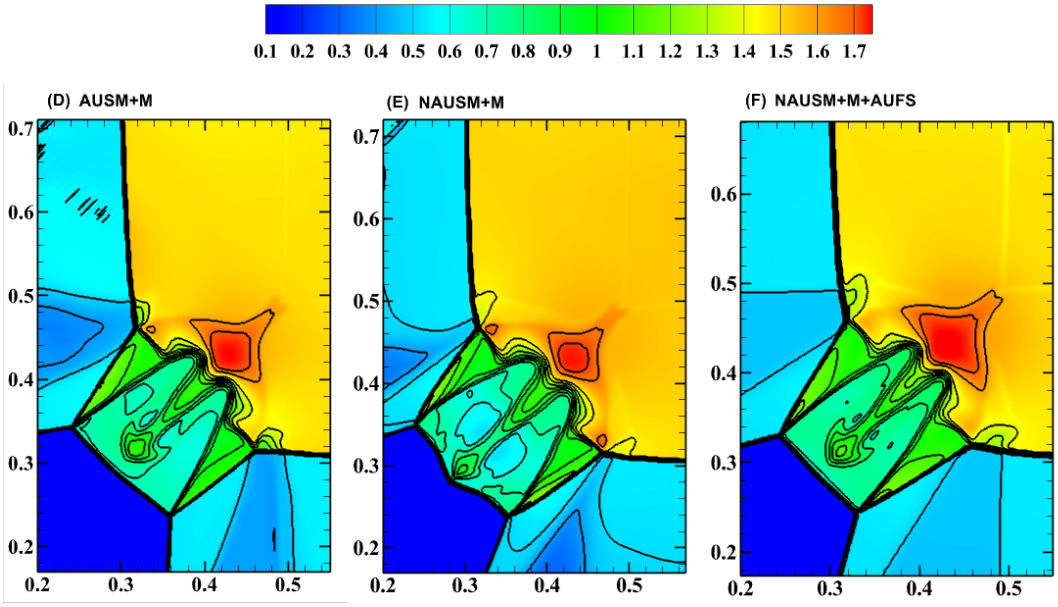

b) Local Enlargement of density contours ((D) AUSM+M, (E) NAUM+M, (F) NAUM+M+AUFS).

Figure 10: Two-dimensional Riemann problem density at t=0.3
(a) Density contours (b) Local Enlargement of density ontours around interaction of shocks.

4.5. Raleigh–Taylor instability

The Rayleigh–Taylor instability (RTI) occurs at the interface between two fluids of different densities when an acceleration is directed from the denser fluid towards the lighter one. In nature, RTI can be observed in volcanic eruptions where lighter gases rise through denser ash layers,

forming mushroom clouds, and in supernova explosions, where expanding core gases interact with denser shells, leading to complex mixing patterns [51]. Industrially, RTI is critical in nuclear fusion, influencing fuel layer mixing during inertial confinement fusion (ICF), and in die casting, where it can cause defects by preventing proper filling if air is trapped above liquid metal [52, 53]. It also plays a role in oceanic mixing and cloud formation, impacting climate and weather patterns [51].

The computational domain spans [0,1/4]×[0,1] and discretized by the grid size of $\Delta x = \Delta y = 1/480$. Initially, the interface is located at y = 1/2, with the denser fluid (density ρ = 2) positioned below the interface and the lighter fluid (density ρ = 1) above, while gravitational acceleration acts in the positive y-direction. The pressure, p, is continuous across the interface. Specifically, for $0 \leq y < 1/2$, the conditions are $\rho = 2$, u = 0, p = 2y + 1, and v = 0.025 cos(8πx); for $1/2 < y \leq 1$, the conditions are $\rho = 1$, u = 0, p = y + 3/2, and v = 0.025c cos(8πx), where c is the sound speed, and the ratio of specific heats is $\gamma = 5/3$. Reflective boundary conditions are imposed on the left and right boundaries. At the top boundary, the conditions are ρ = 1, p = 2.5, and $u = v = 0$, while at the bottom boundary, the conditions are ρ = 2, p = 1, and $u = v = 0$. To simulate the effect of gravitational force a source term, ρ, is added to the right-hand side of the momentum equation, and ρv is added to the energy equation. The simulation is conducted over a time span of t = 1.95, and the results are obtained accordingly.

Figure 11(A–D) presents a comparison of the density contours obtained through the second-order accuracy.The AUFS scheme demonstrates poor performance in resolving contact discontinuities due to its inherently high dissipation characteristics. This excessive dissipation leads to a smoothing of sharp transitions between fluid densities, resulting in a less accurate representation of the fine structures typically associated with RTI, such as the mushroom-shaped spikes. Consequently, the AUFS scheme's resolution is suboptimal for capturing intricate features of the fluid interface. In contrast, the AUSM+M and NAUSM+M schemes exhibit better contact resolution but fail to preserve the symmetry of the fluid profile. These schemes produce more pronounced mushroom-shaped spikes at the interface between the lighter and denser fluids; however, the lack of symmetry suggests inaccuracies in the modeling of the instability. The asymmetry and inaccurate spike formations indicate that these methods are not as effective in capturing the fine balance of forces and mixing patterns present in RTI simulations.

The NAUSM+M+AUFS scheme achieves a notably better resolution of the complex solution structures. It more accurately captures the expected physical behavior, including the symmetry and proper spike formation, which are critical for accurately simulating RTI. This scheme's results closely resemble the fifth-order WENO solution [54].

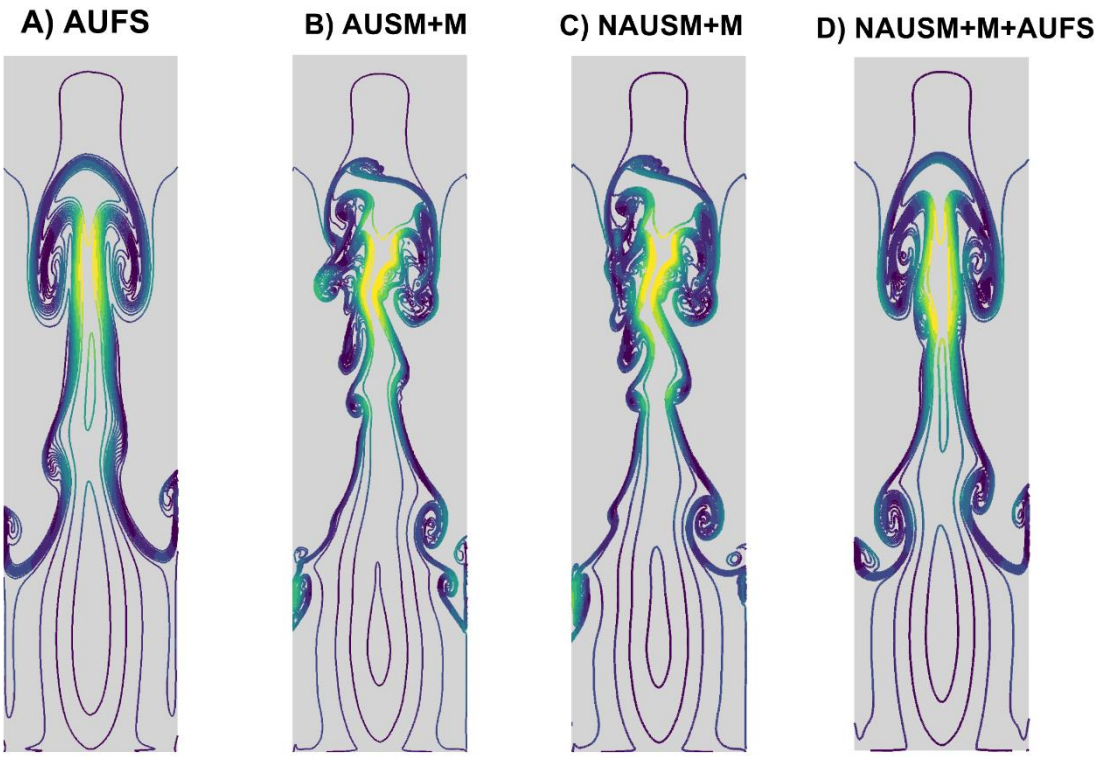

Figure 11: Density contours for Raleigh–Taylor instability problem: (A) AUFS, (B) AUM+M, (C) NAUM+M, (D) NAUM+M+AUFS (15 equally spaced contours from 0.952269 to 2.14589).

5.Conclusion

This research presents the NAUSM+M+AUFS scheme, a novel hybrid numerical method that addresses critical challenges in the simulation of compressible flows on triangular grids. By seamlessly integrating the strengths of NAUSM+M and AUFS, and introducing innovative formulations for interfacial numerical sound velocity and pressure flux dissipation, this scheme effectively enhances shock-capturing capabilities while mitigating common numerical anomalies. Results confirm that the NAUSM+M+AUFS scheme excels in preserving the integrity of shock waves and eliminating the carbuncle phenomenon, particularly in high Mach number and hypersonic flows. The dynamic switching mechanism between AUSM+M and AUFS based on

local flow conditions ensures an optimal balance between accuracy and stability, resulting in improved convergence rates and computational efficiency across various test cases.

The implications of these results are significant for the field of computational fluid dynamics (CFD). The NAUSM+M+AUFS scheme offers a robust and versatile tool for simulating complex, high-speed aerodynamic flows with greater precision and reliability. This advancement has the potential to drive improvements in critical applications such as aerodynamics and propulsion systems, where accurate flow predictions are essential for optimizing performance and safety. However, it is important to acknowledge that the present study has focused solely on structured triangular grids, which limits the general applicability of the method to more complex grid topologies frequently encountered in real-world engineering problems. This constitutes a key limitation of the current work. As such, future research should focus on extending the NAUSM+M+AUFS scheme to hybrid grids that incorporate both triangular and quadrilateral elements. This extension would allow the method to be applied more flexibly to complex geometries and improve its versatility in broader CFD applications.

Further research should focus on exploring the application of this scheme in viscous and turbulent flow scenarios, including both triangular and quadrilateral elements, which will be crucial for further validation.

In summary, the NAUSM+M+AUFS scheme marks a significant leap forward in numerical methods for compressible flow simulation. Its innovative approach not only addresses existing limitations but also sets a new standard for accuracy, stability, and efficiency in CFD, paving the way for future advancements in the field.

References

1. Godounov, S., A difference method for numerical calculation of discontinuous solutions of the equation of hydrodynamics. Matematicheskii Sbornik, 1959. 47(89-3): p. 271-306.
2. Djavareshkian, M.H., M. Moghadas Khorasani, and A. Mohammadi, Comparing the performance of preconditioning matrixes in wide range of internal and external flows. Fluid Mechanics & Aerodynamics, 2022. 10(2): p. 35-54.
3. Khorasani, M.M., A. Mohammadi, and M.H. Djavareshkian, Enhancing convergence and accuracy: A comparative study of preconditioning for steady, laminar, and high gradient ows over a wide range of Mach numbers. International Journal of Modern Physics C, 2024. 2450115: p. 35.
4. Toro, E.F., M. Spruce, and W. Speares, Restoration of the contact surface in the HLL-Riemann solver. Shock waves, 1994. 4: p. 25-34.
5. Osher, S. and F. Solomon, Upwind difference schemes for hyperbolic systems of conservation laws. Mathematics of computation, 1982. 38(158): p. 339-374.
6. Moghadas Khorasani, M. and M.H. Djavareshkian, Enhancing accuracy and efficiency: A novel implicit–explicit approach for fluid dynamics simulation. Physics of Fluids, 2024. 36(3).
7. Harten, A., P.D. Lax, and B.v. Leer, On upstream differencing and Godunov-type schemes for hyperbolic conservation laws. SIAM review, 1983. 25(1): p. 35-61.
8. Rusanov, V.V., The calculation of the interaction of non-stationary shock waves with barriers. Z. Vycisl. Mat. i Mat. Fiz, 1961. 1: p. 267-279.
9. Van Leer, B. Flux-vector splitting for the Euler equations. in Eighth International Conference on Numerical Methods in Fluid Dynamics: Proceedings of the Conference, Rheinisch-Westfälische Technische Hochschule Aachen, Germany, June 28–July 2, 1982. 2005. Springer.
10. Steger, J.L. and R. Warming, Flux vector splitting of the inviscid gasdynamic equations with application to finite-difference methods. Journal of computational physics, 1981. 40(2): p. 263-293.
11. Liou, M.-S. and C.J. Steffen Jr, A new flux splitting scheme. Journal of Computational physics, 1993. 107(1): p. 23-39.
12. Wada, Y. and M.-S. Liou, An accurate and robust flux splitting scheme for shock and contact discontinuities. SIAM Journal on Scientific Computing, 1997. 18(3): p. 633-657.
13. Liou, M.-S., A sequel to ausm: Ausm+. Journal of computational Physics, 1996. 129(2): p. 364-382.
14. Kim, K.H., C. Kim, and O.-H. Rho, Methods for the accurate computations of hypersonic flows: I. AUSMPW+ scheme. Journal of computational physics, 2001. 174(1): p. 38-80.
15. Liou, M.-S., A sequel to AUSM, Part II: AUSM+-up for all speeds. Journal of computational physics, 2006. 214(1): p. 137-170.
16. Chen, S.-s., et al., Affordable shock-stable item for Godunov-type schemes against carbuncle phenomenon. Journal of Computational Physics, 2018. 373: p. 662-672.
17. Rodionov, A.V., Artificial viscosity in Godunov-type schemes to cure the carbuncle phenomenon. Journal of Computational Physics, 2017. 345: p. 308-329.
18. Li, X.-s. and C.-w. Gu, Mechanism of Roe-type schemes for all-speed flows and its application. Computers & Fluids, 2013. 86: p. 56-70.

19. Qu, F., D. Sun, and C. Yan, A new flux splitting scheme for the Euler equations II: E-AUSMPWAS for all speeds. Communications in Nonlinear Science and Numerical Simulation, 2018. 57: p. 58-79.
20. Qu, F., et al., Self-similar structures based genuinely two-dimensional Riemann solvers in curvilinear coordinates. Journal of Computational Physics, 2020. 420: p. 109668.
21. Shima, E. and K. Kitamura, Parameter-free simple low-dissipation AUSM-family scheme for all speeds. AIAA journal, 2011. 49(8): p. 1693-1709.
22. Kitamura, K. and E. Shima, Towards shock-stable and accurate hypersonic heating computations: A new pressure flux for AUSM-family schemes. Journal of Computational Physics, 2013. 245: p. 62-83.
23. Shima, E. and K. Kitamura. On new simple low-dissipation scheme of AUSM-family for all speeds. in 47th AIAA Aerospace Sciences Meeting Including the New Horizons Forum and Aerospace Exposition. 2009.
24. Chakravarthy, K. and D. Chakraborty, Modified SLAU2 scheme with enhanced shock stability. Computers & Fluids, 2014. 100: p. 176-184.
25. Chen, S.-s., et al., An improved AUSM-family scheme with robustness and accuracy for all Mach number flows. Applied Mathematical Modelling, 2020. 77: p. 1065-1081.
26. Mohammadi, A. and M.H. Djavareshkian, Modified advection upstream splitting method: Revolutionizing accuracy and convergence speed in low-Mach flows. Physics of Fluids, 2023. 35(10).
27. Mohammadi, A. and M.H. Djavareshkian, Advancing high-speed flow simulations: SAUSM—An innovative hybrid numerical scheme for shock stability and accuracy. Int. J. Mod. Phys. C, 2023. 35: p. 2450045.
28. Kaewta, S., et al., A comparison of TVD limiter functions for a convection–diffusion–reaction equation and Euler equations on triangular grids. Journal of the Brazilian Society of Mechanical Sciences and Engineering, 2022. 44(11): p. 500.
29. Hedayati Nasab, S., Accelerated Temporal Schemes for High-Order Unstructured Methods. 2021, Concordia University.
30. Quirk, J.J., A contribution to the great Riemann solver debate. 1997: Springer.
31. Phongthanapanich, S., A parameter-free AUSM-based scheme for healing carbuncle phenomenon. Journal of the Brazilian Society of Mechanical Sciences and Engineering, 2016. 38: p. 691-701.
32. Liou, M.-S., Mass flux schemes and connection to shock instability. Journal of Computational Physics, 2000. 160(2): p. 623-648.
33. Zhang, F., et al., A robust low-dissipation AUSM-family scheme for numerical shock stability on unstructured grids. International Journal for Numerical Methods in Fluids, 2017. 84(3): p. 135-151.
34. Phongthanapanich, S., An accurate and robust AUSM-family scheme on two-dimensional triangular grids. Shock Waves, 2019. 29(5): p. 755-768.
35. Phongthanapanich, S., A stable hybrid Roe scheme on triangular grids. International Journal for Numerical Methods in Fluids, 2021. 93(4): p. 978-1000.
36. Phongthanapanich, S., A. Matthujak, and K. Ohtani, Accurate and robust hybrid HLLC Riemann solver on triangular grids. AIAA Journal, 2023. 61(9): p. 3935-3957.
37. Javareshkian, M. and A. Mohammadi, nvestigation of a Broad category Of AUSM Family in the 1D and 2D Unsteady Flows. Journal of Solid and Fluid Mechanics, 2020. 10(4): p. 303-315.

38. Sun, M. and K. Takayama, An artificially upstream flux vector splitting scheme for the Euler equations. Journal of Computational Physics, 2003. 189(1): p. 305-329.
39. Edwards, J.R. and M.-S. Liou, Low-diffusion flux-splitting methods for flows at all speeds. AIAA journal, 1998. 36(9): p. 1610-1617.
40. Qu, F., et al., A parameter-free upwind scheme for all speeds' simulations. Science China Technological Sciences, 2015. 58: p. 434-442.
41. Soltani, M., J. Younsi, and M. Farahani, Investigation of a new flux scheme for the numerical simulation of the supersonic intake flow. Proceedings of the Institution of Mechanical Engineers, Part G: Journal of Aerospace Engineering, 2012. 226(11): p. 1445-1454.
42. Liu, L., X. Li, and Z. Shen, Overcoming shock instability of the HLLE-type Riemann solvers. Journal of Computational Physics, 2020. 418: p. 109628.
43. Simon, S. and J. Mandal, A simple cure for numerical shock instability in the HLLC Riemann solver. Journal of Computational Physics, 2019. 378: p. 477-496.
44. Fukushima, G. and K. Kitamura, Improved hybrid approach of monotonic upstream-centered scheme for conservation laws and discontinuity sharpening technique for steady and unsteady flows. Physics of Fluids, 2024. 36(4).
45. Toro, E.F., Riemann Solvers and Numerical Methods for Fluid Dynamics [electronic resource]: A Practical Introduction.
46. Tan, S., L. Hu, and H. Yuan, Development of a shock-stable and contact-preserving scheme for multidimensional Euler equations. AIAA Journal, 2022. 60(9): p. 5232-5248.
47. Peery, K. and S. Imlay. Blunt-body flow simulations. in 24th joint propulsion conference. 1988.
48. Phongthanapanich, S., et al., A shock-stable rotated-hybrid Riemann solver on rectangular and triangular grids. Physics of Fluids, 2024. 36(4).
49. Liska, R. and B. Wendroff, Comparison of several difference schemes on 1D and 2D test problems for the Euler equations. SIAM Journal on Scientific Computing, 2003. 25(3): p. 995-1017.
50. Lax, P.D. and X.-D. Liu, Solution of two-dimensional Riemann problems of gas dynamics by positive schemes. SIAM Journal on Scientific Computing, 1998. 19(2): p. 319-340.
51. Singh, S., et al., Plasma Waves and Rayleigh–Taylor Instability: Theory and Application, in Plasma Science-Recent Advances, New Perspectives and Applications. 2023, IntechOpen.
52. Cook, A.W. and D. Youngs, Rayleigh-Taylor instability and mixing. Scholarpedia, 2009. 4(2): p. 6092.
53. Ramaprabhu, P., V. Karkhanis, and A.G. Lawrie, The Rayleigh-Taylor Instability driven by an accel-decel-accel profile. Physics of Fluids, 2013. 25(11).
54. Xu, Z. and C.-W. Shu, Anti-diffusive flux corrections for high order finite difference WENO schemes. Journal of Computational Physics, 2005. 205(2): p. 458-485.